Performance of Multi Chamber Oscillating Water Columns: Effects of Chamber Configuration and Power Absorption

Adnan Sandy Dwi Marta[1,2,*], Agus Wibowo[1], Bondan Fiqi Riyalda[1], Fuad Darul Muttaqin[1], Amar Makruf Tinulad Fil Ardli[1], Amien Rusdiutomo[1], Wahyu Hendriyono[2], Affandy Hamid[2], Qidun Maulana Binu Soesanto[3], Ristiyanto Adiputra[2]

[1]Directorate of Laboratory Management, Research Facilities, and Science and Technology Park, National Research and Innovation Agency, Indonesia
[2]Research Center for Hydrodynamics Technology, National Research and Innovation Agency, Indonesia
[3]Research Center for Energy Conversion and Conservation, National Research and Innovation Agency, Indonesia

*Author to whom correspondence should be addressed:
E-mail: adna001@brin.go.id

(Received May 28, 2025; Revised August 04, 2025; Accepted December 17, 2025)

Abstract: Oscillating Water Column (OWC) is a promising green energy technology for wave energy conversion, accounting for 26.79% of global wave energy converter applications. This study investigates the hydrodynamic and aerodynamic performance of multi-chamber OWC systems with variations in chamber inclination angles (0°, 20°, and 40°) and the number of chambers (2, 3, and 4). Computational Fluid Dynamics (CFD) simulations were performed using the Reynolds-Averaged Navier-Stokes (RANS) equations and the RNG turbulence model to analyze flow characteristics under regular wave conditions. Key parameters evaluated include free surface elevation, air pressure, air velocity, power distribution, and power absorption. Results indicate that the highest free surface elevation (1.545 m) occurred in a 4-chamber configuration with a 0° inclination. The maximum air pressure (774,804 Pa), air velocity (36.356 m/s), and power distribution (23.58 kWh) were found in a 3-chamber system with a 40° inclination. Meanwhile, the highest total power absorption (42.79 kWh) was observed in a 4-chamber system with a 40° inclination. The 4-chamber configuration with a 40° inclination showed the best performance, achieving 42.79 kWh of power and 0.86 efficiency—outperforming 3-cahmber and 2-chamber setups by 52% and 77%, respectively. Generally, configurations with more chambers resulted in greater power absorption but lower individual pressure and velocity peaks. Increased inclination tends to reduce water surface oscillation. These findings provide insights for optimizing multi-chamber OWC design for improved wave energy capture.

Keywords: inclination; multi-chamber; OWC; power absorption; wave energy converter

1. Introduction

Indonesia's rising energy demand may push CO2 emissions beyond 1.3 billion tons by 2060, urging a shift to renewables[1)]. Wave energy is an emerging renewable source with significant potential, particularly for coastal nations[2)]. Although less mature than wind[3,4)], solar[5-7)] and geothermal[8,9)] technologies, the Oscillating Water Column (OWC) has become the most developed and widely studied wave energy conversion method[10)]. OWC systems represent approximately 26.79% of global wave energy converter implementations and, when optimally configured, can generate electricity at scales ranging from kilowatts to megawatts[11)].

The OWC system comprises two main components: a wave-capturing chamber and an electric generator. The submerged chamber features an opening below the water surface, allowing it to harness the vertical motion of ocean waves[12)]. Globally, Japan began pioneered the technology with a 40 kW power buoy in 1983 and a 60 kW breakwater-integrated system in 1990[13,14)]. Other notable developments include a 500 kW shoreline-mounted spar buoy built by Norway in 1985[15)], and a 100 kW fixed OWC

Cite: A. Marta et al., "Performance of Multi Chamber Oscillating Water Columns: Effects of Chamber Configuration and Power Absorption". Evergreen, 13 (01) 173-187 (2026). https://doi.org/10.5109/7407643.

developed by China between 1989 and 1991 in Shanwei City[16,17].

In 1990, India tested a 125 kW OWC system in Trivandrum, initially using a wells turbine, which was later replaced with an impulse turbine[18]. In the same year, a full-scale fixed structure was built in Vizhinjam, operating seasonally at 75 kW (April–November) and 25 kW (December–March)[19,20]. Between 1998 and 2001, Japan developed the Mighty Whale project, featuring a 110 kW three-chamber floating OWC tested in Gokasho Bay[21].

In 1999, Portugal built a 400 kW fixed OWC system on Pico Island, Azores, using a design similar to Japan's Mighty Whale[15]. Australia followed with the Energetech project in 2002, developing a 500 kW fixed-structure OWC[22]. In 2007, Japan constructed a small-scale OWC at Niigata Port with a 450 kW rated output and a peak of 880 kW[23,24].

In 2008, Ireland developed a 2:4 scale floating Backward Bent Duct Buoy (BBDB) in Galway Bay under the CORES project, generating 13 kW[25]. In 2011, Spain built and installed a 296 kW OWC integrated into the breakwater at Mutriku Port, which remains operational to this day[26].

Scotland followed in 2012 with the LIMPET project, building a 500 kW shore-based OWC on Islay Island, later downgraded to 250 kW[27]. Italy introduced the REWEC3 system in 2016, constructing a 25 kW U-shaped OWC integrated into Civitavecchia Harbour's breakwater, with a total installed capacity nearing 2.5 MW, still in operation[28,29]. In 2017, South Korea completed a 500 kW bottom-fixed OWC at Yongsoo, Jeju Island[30].

The historical development of OWC systems across various countries reflects a growing global interest in wave energy as a reliable source of coastal electricity. These projects have demonstrated OWC's technical feasibility and its contribution to sustainable energy supply[31]. Following this progress, recent studies emphasize the importance of OWC geometry, as structural parameters such as chamber size, shape, number, and layout—significantly influence the efficiency of wave energy conversion[32],

Multi-chamber OWC systems offer significant technical solutions to the shortcomings of single-chamber systems in terms of efficiency, flexibility, and reliability. Their primary advantages include broad-spectrum wave energy capture, reduced internal interference, and system resilience to dynamic sea conditions[33].

Dual-chamber OWC systems have been shown to outperform single-chamber configurations, offering significantly higher peak energy absorption and a capture width ratio (CWR) nearly three times greater. Modeling and experimental studies report peak efficiency improvements of 8% and 4%, respectively[34- 36].

However, the design of dual-chamber OWCs requires careful consideration of structural integrity and hydrodynamic efficiency. The sea-facing wall, subjected to the greatest loads, must use robust materials, and a narrower width ratio is generally recommended for the sub-chamber[37]. Research on multicolumn configurations indicates superior energy conversion efficiency compared to isolated systems[38].

A nonlinear numerical study on land-based dual-chamber OWC systems found that horizontal wave forces on the outer chamber increase with greater submergence depth[39]. Another comparative analysis of three OWC configurations indicated that dual-chamber setups are less effective at deeper water levels in terms of energy absorption[40].

While scale-model experiments yield more accurate performance data than numerical simulations, they require costly and specialized equipment. Across modeling approaches, the trend in efficiency remains consistent; however, peak values differ significantly. Analytical models suggest up to 90% efficiency, CFD simulations reach about 60%, and physical tests show a maximum of 40%. These discrepancies stem from simplifications in mathematical modeling that fail to capture complex water-air-structure interactions[41].

A numerical model integrating wave-structure hydrodynamics and air chamber thermodynamics has been developed to analyze dual-chamber OWC performance. Wave forces are computed via the boundary element method based on potential flow theory, while airflow behavior is modeled using mass and energy conservation laws. This approach evaluates parameters such as air pressure, reflection coefficient, and both individual and overall energy conversion efficiencies by solving boundary integral equations. The model also investigates the influence of design variables including nozzle ratio, water depth, curtain wall depth, and forespace width[42].

Wang et al. (2019) employed a 2D OpenFOAM-based numerical model and reported hydrodynamic efficiency reaching 80%, though the accuracy varies across wave frequencies[43]. Similarly, Abbasnia et al. (2021) introduced a fully nonlinear adaptive model that incorporates compressible air dynamics for improved realism[44] Shalby et al. (2019) conducted 3D CFD simulations using STAR-CCM+ on a small-scale multi-chamber OWC, achieving close agreement with experimental data across multiple performance metrics[45].

Compared to physical experiments, CFD simulations offer substantial advantages—such as eliminating large-scale setups, enabling continuous operation, and reducing costs and time requirements with proper computational resources[46]. This study aims to perform a comparative analysis of free surface elevation, air pressure, air velocity, power distribution, and energy absorption in multi-chamber OWC systems, focusing on the influence of different chamber configurations and inclination angles. The configurations include systems with two, three, and four chambers, each tested at inclination angles of 0°, 20°,

and 40°.

Research developments in Oscillating Water Columns (OWCs) indicate a shift from single-chamber to multi-chamber systems to improve wave energy efficiency. Single-chamber systems were initially used due to their simple design, but they were limited to a narrow frequency range and had low efficiency. To address this, developed a dual-chamber system, which was proven to increase pneumatic efficiency by up to 8% and expand the operating frequency range. Subsequently, experimentally tested a triple-chamber OWC and found increased power output and air pressure stability. Most recently, Ning et al. (2024) studied a system with up to five chambers, which increased cumulative power but decreased individual chamber efficiency due to flow interference. Optimizing the number of chambers and geometry is now the focus of further research[47, 48)]

This study will address research gaps in previous studies related to the comparative analysis of free surface elevation, air pressure, air velocity, power distribution, and energy absorption in multi-chamber OWC systems, focusing on the effects of different chamber configurations and tilt angles. These configurations include systems with two, three, and four chambers, tested at tilt angles of 0°, 20°, and 40°, respectively.

The analysis is conducted through Computational Fluid Dynamics (CFD) simulations, employing the Reynolds-Averaged Navier-Stokes (RANS) equations coupled with the Renormalization Group (RNG) turbulence model to resolve flow characteristics. Wave dynamics are modeled using second-order Stokes theory, while the Volume of Fluid (VOF) method captures the air–water interface with a two-phase flow approach.

2. Numerical methods

2.1. Governing equation

This study implements numerical computational simulation using Computational Fluid Dynamics (CFD) software, namely the FLOW 3D™ application. The parameters and equations used in the numerical simulation have been validated against experimental data conducted by Supriyanto et al.[49)]. The Navier-Stokes equations used in these simulations describe the behavior of an incompressible Newtonian fluid, having the following vector notation[50,51)]:

$$\rho\left(\frac{\partial v}{\partial t} + v.\nabla v\right) = \nabla P + \mu\nabla^2 v + \rho g \quad (1)$$

$$\nabla . v = 0 \quad (2)$$

Based on the formula above, ρ is the fluid density, P is the pressure, and v is the velocity. ∂t is the time, ∇ is the Laplacian vector, μ is the dynamic viscosity, and g is the acceleration due to gravity. The RNG turbulence model used in this numerical computational simulation aims to calculate the parameters related to the average turbulence, namely turbulent energy, and dissipation rate[49)].

The constants of the RNG model are found through theoretical derivation, while the constants in the k-ε model come from experimental evidence. In the low-intensity turbulence and shear fluid regions, FLOW 3DTM will produce more accurate results using the RNG model. To represent and manage the turbulent effects more precisely, the k-ε renormalization group (RNG) turbulence model will also be used. The governing equations of the k-ε RNG model are written as follows[52-54)]:

$$\frac{\partial(\rho k)}{\partial t} + \frac{\partial(\rho k u_i)}{\partial x_i}\left[\left(\mu + \frac{\mu_t}{\sigma_k}\right)\frac{\partial k}{\partial x_j}\right] + P_k - \rho\epsilon \quad (3)$$

$$\frac{\partial(\rho \epsilon)}{\partial t} + \frac{\partial(\rho \epsilon u_i)}{\partial x_i}\left[\left(\mu + \frac{\mu_t}{\sigma_\epsilon}\right)\frac{\partial k}{\partial x_j}\right] + C_{1\epsilon}\frac{\epsilon}{k}P_k - C^*_{2\epsilon}\rho\frac{\epsilon^2}{k} \quad (4)$$

RNG was chosen because it is superior in handling large-scale turbulence, vortices, and air-water interactions in OWC. This model includes additional corrections for high-strain flow, improving accuracy in multi-chamber systems. RNG is more stable in large fluid domains and better at capturing flow separation and vortices. The density and viscosity at the grid interface can be determined by using the volume fractions of the two phases, which can then be applied to the momentum equation[55)].

The k-ε RNG can be used with coarser meshes (y^+ values between 30–300), making it suitable for large-scale simulations with limited resources. Meanwhile, the k-ω SST model is superior for flows with flow separation and boundary-layer transitions, but requires a finer mesh and longer computation time. These two models are used separately, as each is designed for different flow conditions, except in hybrid models such as SST that combine the advantages of both k-ω and k-ε. The k-ε RNG is more stable in large domains and complex flows with a coarse mesh[56,57)]

The free surface grids corresponding to the density and viscosity are contained in the equation:

$$\rho = f_0\,\rho_0 + f_1\,\rho_1 \quad (5)$$

$$v = f_0\,v_0 + f_1\,v_1 \quad (6)$$

where ρ is the fluid density, ν is the kinematic viscosity, and f is the volume fraction, while water is represented by subscript 0 and air is represented by subscript 1.

In this numerical computational simulation, water and air are combined (both fluids). The VOF method involving two different fluids is used to analyze the OWC[58,59)].

The free surface elevation will be tracked and the contact between air and water will be predicted using the VOF approach[59)]. The volume fraction controlled by the

expression equation is as follows:

$$\frac{\partial f_m}{\partial t} + \nabla.(f_m.U) = 0 \qquad (7)$$

where fm is the volume fraction bounded by $0 \leq f_m \leq 1$; $f_m = 1$ indicates that the grid is completely filled with fluid m^{th}, $f_m = 1$ indicates that there is no fluid m^{th} in the grid, and $0 < f_m < 1$ describes the presence of an interface between water and air. ∇ is the Laplacian vector and U is the velocity field[49].

2.2. Boundary condition in multi chamber model

The simulation area is broken down into box-like or rectangular grid pieces using a technique called Cartesian meshing, which is based on the Cartesian coordinate system. The impact of the mesh on the geometry is assessed using the Fractional Area Volume Obstacle Representation (FAVOR) technique[60].

Figure 1. shows the four key conditions that make up the boundary conditions. The length of the 3D CFD wave flume follows the HYDRALAB guidelines[61]. The simulated wall's width is aligned with that of the test model, denoting it as the lower boundary. The wall boundary conditions are no-slip and no-penetration, as implemented by Trivedi et al. (2023)[62].

The channel sides are defined as symmetric (S), which means that the physical geometry, flow pattern, and thermal solution are expected to show symmetric characteristics. The outflow is the area where water can overshoot, leading to a decrease in the discharge amount. The upstream inlet condition changes with the wave height and period, indicated by the symbol (WV). The upper boundary condition specifies a free surface with a fluid fraction of 0.5 and a stagnation pressure (P) of 101325 Pascal to account for air-water interactions.

This simulation was conducted under transient conditions (time-dependent) based on several factors. The wave input follows Airy theory (regular waves), representing periodic stable waves. The OWC model is positioned 3L from the wave input, following Hydralab III guidelines to ensure the waves are fully developed before reaching the system. The upper boundary condition uses a specified pressure - open channel with sufficient height to prevent reflection and interference effects. With these parameters, the simulation ensures the system reaches a convergence (the system results show no significant changes), allowing for a stable analysis of OWC performance.

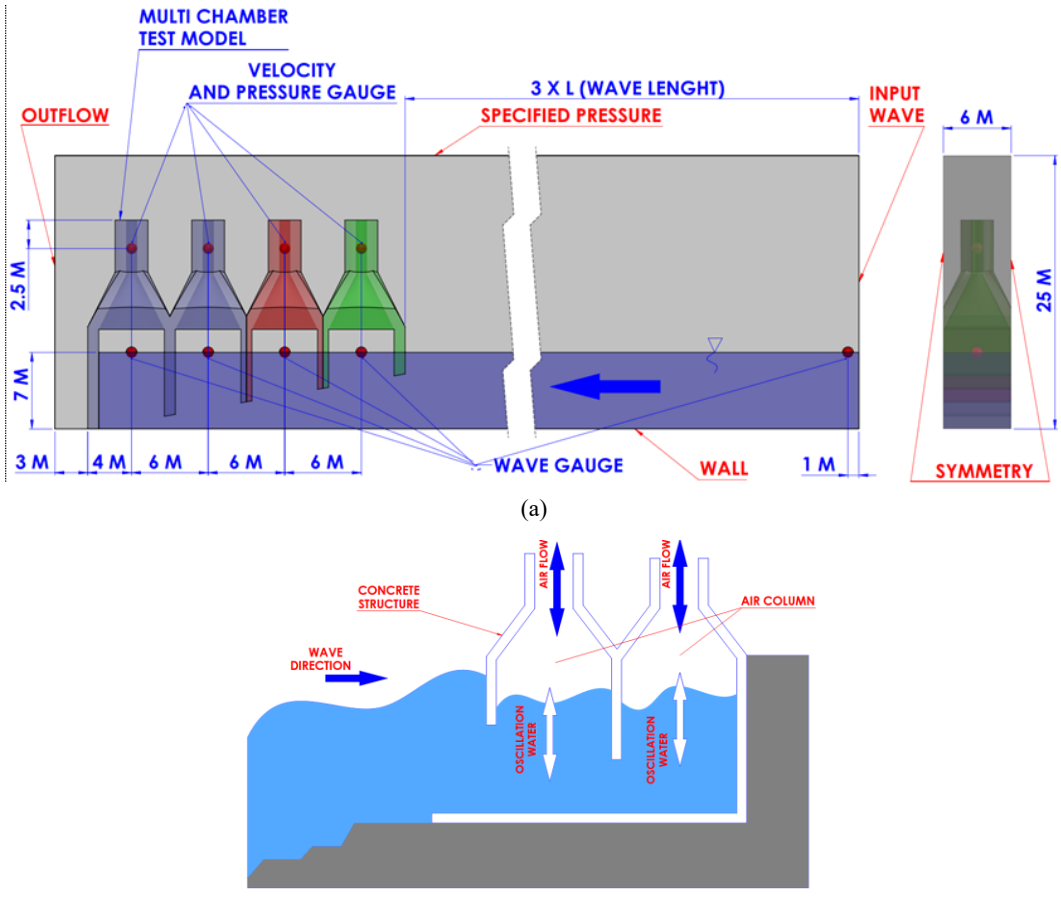

Fig. 1: (a) Boundary condition model and gauge setup in multi chamber; (b) schematic diagram of the system

Cite: A. Marta et al., "Performance of Multi Chamber Oscillating Water Columns: Effects of Chamber Configuration and Power Absorption". Evergreen, 13 (01) 173-187 (2026). https://doi.org/10.5109/7407643.

The linear wave theory of George Biddell Airy is used as the basis model to generate regular waves at the mesh boundary as input. It is assumed that these linear waves enter the computational domain from a flat-bottomed reservoir. Linear waves are characterized by wave number ($k=2\pi/\lambda$), wave frequency (ω), wavelength (λ), and wave amplitude (A). The vertical coordinate of the wave-free surface height, represented as $z = \eta(x,t)$, describes the wave[63].

$$\eta = A \cos(kx - \omega t + \varphi) \quad (8)$$

The wave amplitude (A) is smaller than the water depth (h), where φ represents the phase shift angle. The wave velocity $c = \omega/k$ is expressed as:

$$c^2 = \frac{g\lambda}{2\pi} tanh\ \frac{2\pi h}{\lambda} \quad (9)$$

Figure 1 is one of the views of the meshing and geometry model settings in multi-space. There is a wave gauge placement in front of the wave generator, which functions to ensure that the wave height is following the desired height. The direction of the blue arrow explains the direction of the wave flow coming from the generator. The wave gauge is positioned in each chamber to determine the height of the water surface in each chamber or duct when the simulation is carried out. While the velocity and pressure gauges are positioned on the neck of the chamber, to determine the velocity and wind pressure values from each chamber or duct.

The validation involved comparing the experimental results with numerical simulations. The mesh independence study, as shown in Figure 2, was conducted to determine the optimal mesh size for the simulation, ensuring that the results are not dependent on the mesh resolution. This study indicates that a mesh size smaller than 0.36 is suitable for achieving stable and accurate results. Based on these criteria, a mesh size of 0.32 was selected for the simulation, as it falls within the optimal range identified by the independence study. This selection ensures a balance between computational accuracy and efficiency in computation time.

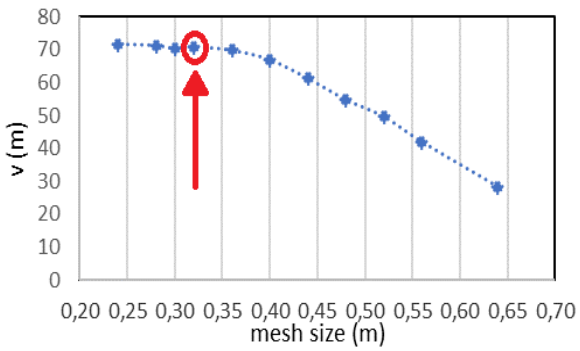

Fig. 2: Mesh independence study

The selection of parameters (Table 1) is based on the power generated by the OWC multi-chamber system. The number of chambers (2, 3, 4) was chosen to evaluate the impact of increasing chambers on wave energy conversion power. The chamber inclination (0°, 20°, 40°) was used to understand how angle variations affect flow patterns and air pressure in the system. 0° serves as the baseline, while 20° and 40° examine the effects of gradual inclination. This combination enables the optimization analysis of the OWC design to enhance wave energy conversion performance.

2.3. Test multi chamber model

Figure 3 shows the multi chamber model used in this study. Figure 3a displays the detailed design of the multi chamber variation with 2, 3, and 4 chambers in the OWC system, including the different incline angles and variation angles 0˚, 20˚, and 40˚ that were tested in this research. Figure 3b presents a complete three-dimensional view of the multi chamber OWC design, helping to understand its structure and arrangement better. Figure 3 shows a multi chamber OWC, with chamber 1 being named Duct1, chamber 2 being Duct2, chamber 3 being Duct3, and chamber 4 being Duct4.

3. Result and discussion

Before carrying out the simulation, the following validation steps need to be carried out.

3.1. Validation

To ensure the reliability and accuracy of the simulation results, a validation process was conducted. This sub-section details the validation by directly comparing the CFD results against experimental data, as well as establishing the convergence of the numerical model. The process of validation comprised components where experimental results were matched with numerical simulations. Pressure measurements from the L-shaped chamber and wave measurements from the chamber area were used to validate both numerical and experimental results[64,65]. The validation results correlating to RMSE of 0.07 demonstrate a correlation with the wave heights in the chamber area, as depicted in Figure 4(a).

Differences between the experimental data and numerical simulations occur because the experiment has a mechanical ramp-up period of 10 seconds, during which the input wave gradually develops as per the test scenario

Table 1: Condition for numerical testing

Parameter	Variables
Number of Chamber	Multi chamber : 2, 3, 4
Inclination of Chamber	Degree: 0° ; 20°, 40°
Other parameters: Water depth; wave period; and wave height generation	7 meter; 7 second; and 1 meter

Cite: A. Marta et al., "Performance of Multi Chamber Oscillating Water Columns: Effects of Chamber Configuration and Power Absorption". Evergreen, 13 (01) 173-187 (2026). https://doi.org/10.5109/7407643.

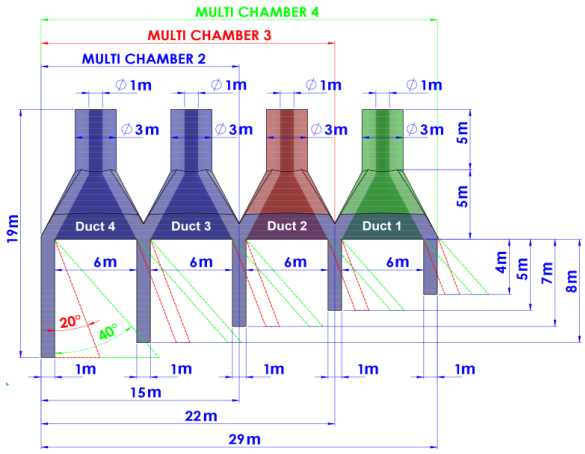

(a)

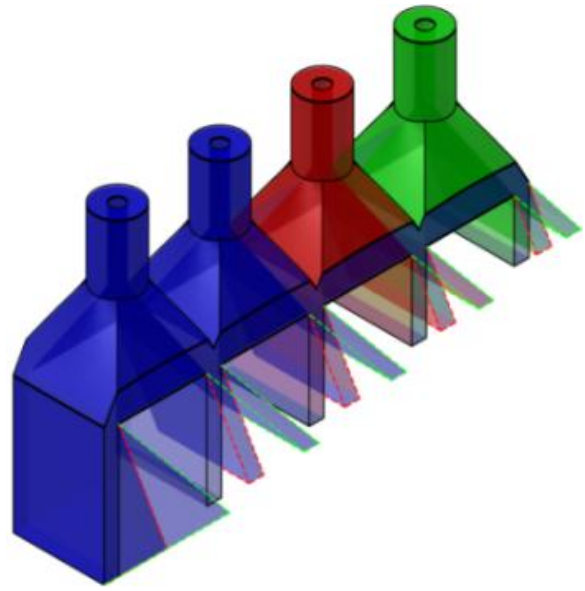

(b)

Fig. 3: The multi chamber model (a) Detail design (b) 3D model with incline

(as shown in the green rectangle in Figure 4(a)). On the other hand, the input wave in the CFD simulation immediately aligns with the test scenario.

To achieve comprehensive validation beyond the isolated wave height in the chamber, a comparison between numerical and experimental differential pressure results was performed. The coefficient of determination, commonly referred to as R-squared (R^2), shown in Figure 4(B), demonstrates how well the numerical results align with the experimental findings for differential air pressure and air velocity. For the pressure difference and airflow velocity comparison, the R^2 values are 0.9993 and 0.9987. These results demonstrate the high consistency and reliability of the numerical simulations when compared to the experimental findings[65].

3.2. Flow visualization in multi chamber OWC

Figure 5 shows the direction of airflow and the shape of water movement. When water enters the chamber, it

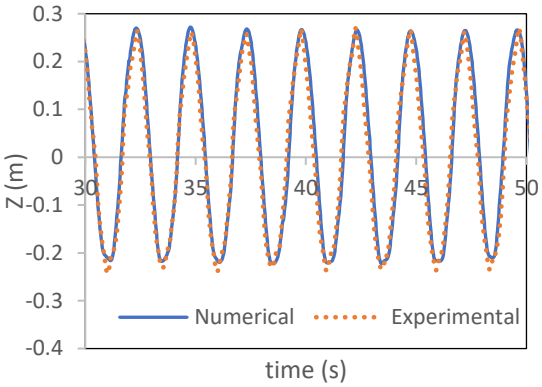

(a)

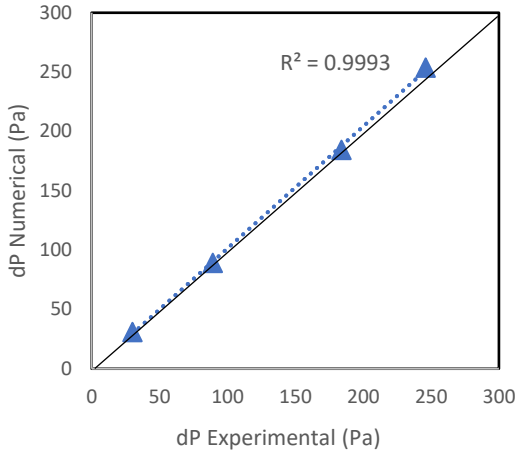

(b)

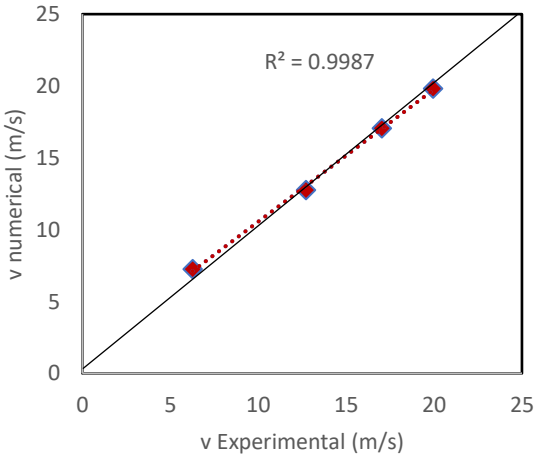

(c)

Fig. 4: (a) Comparison of time series wave height isolation experimentally and numerically. Velocity vector and pressure selected visualization in multi chamber, (b) Results of comparison of differential air pressure experimentally and numerically, (c) Results of comparison of airflow velocity experimentally and numerically.

creates high air pressure inside. This higher pressure makes the air move faster as it leaves the chamber and heads toward the turbine. The Figure also shows how ocean

waves travel through the multi chamber OWC system, causing the water surface to go up and down. When the water level rises inside the chamber, it increases the air pressure, pushing air out. When the water level falls, the pressure drops and air flows back into the chamber. This up-and-down motion happens in each chamber one after the other.

Figure 6 shows that at 34.20 seconds the wave enters the chamber, and then the air velocity in Duct1 increases towards the exit. At the same time, the pressure vector shows an increase towards the exit of Duct1. Furthermore, the wave will enter Duct2, Duct3, and Duct4 when the model is run.

Figure 6(b) displays a view of pressure-selected areas in a multi chamber setup. The smooth pressure lines and water level lines show that the water flow and wave height do not enter the OWC chamber well, and might even bounce back out. This is clear from the swirling flow pattern in front of the OWC and the changing wave height lines, which point to poor performance[66,67]. This poor performance might be due to the chamber's design, the inclination of the chamber walls, and how the waves interact with the chamber's shape.

3.3. Analysis based on number of chambers, inclination, absorption, and optimization.

In Figure 7, it can be seen that the highest Z is in Duct3 in the 4-chamber configuration with an inclination of 0° with a value of 1.545 m. The lowest Z is in Duct4 in the 4-chamber configuration with an inclination of 40° with a value of 0.249 m. In Figure 7, it can also be seen that the highest P is in Duct1 in the 3-chamber configuration with an inclination of 40° with a value of 774.80 Pa. The lowest P is in Duct4 in the multi chamber model with an inclination of 40° with a value of 43.300 Pa. In Figure 7, it can also be seen that the highest v is in Duct1 in the 3-chamber configuration with an inclination of 40° with a

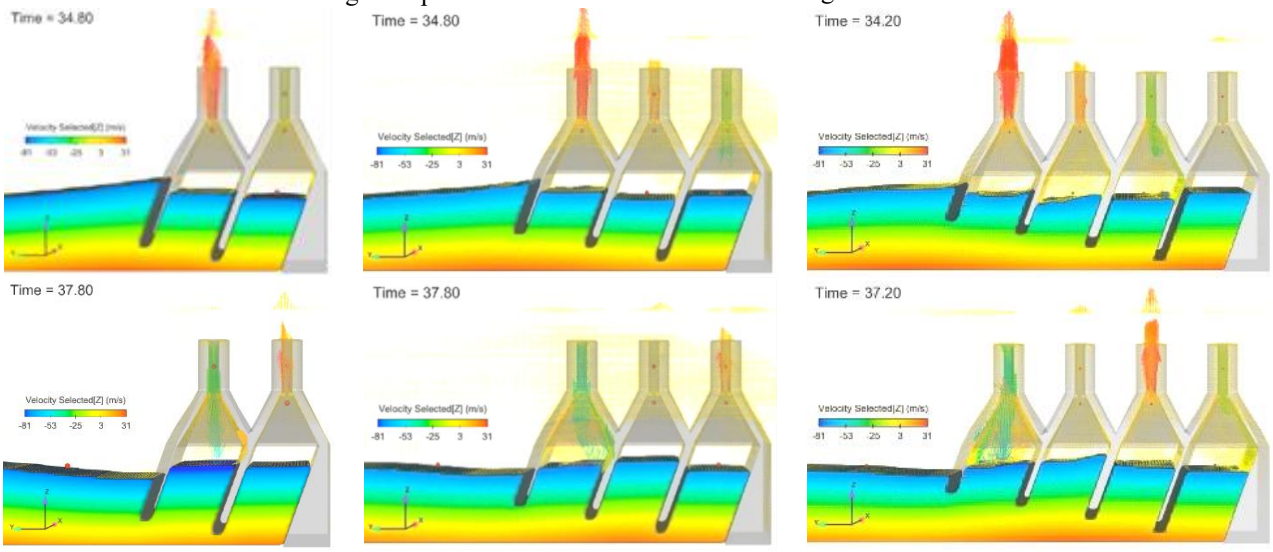

(a) **(b)** **(c)**

Fig. 5: Airflow velocity vector visualization on multi-OWC: (a) 2 chambers, (b) 3 chambers, (c) 4 chambers

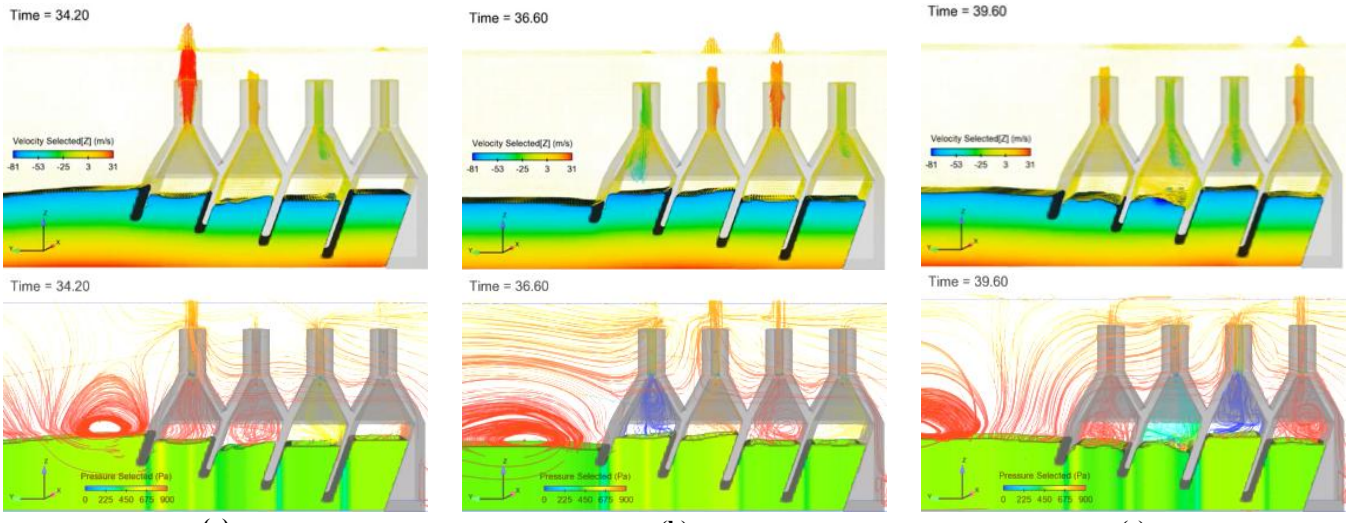

(a) **(b)** **(c)**

Fig. 6: Comparison of airflow velocity vector visualization and air pressure streamline in multi-OWC chamber 4 duct during compression to decompression process: (a) air velocity vector, (b) air pressure streamline

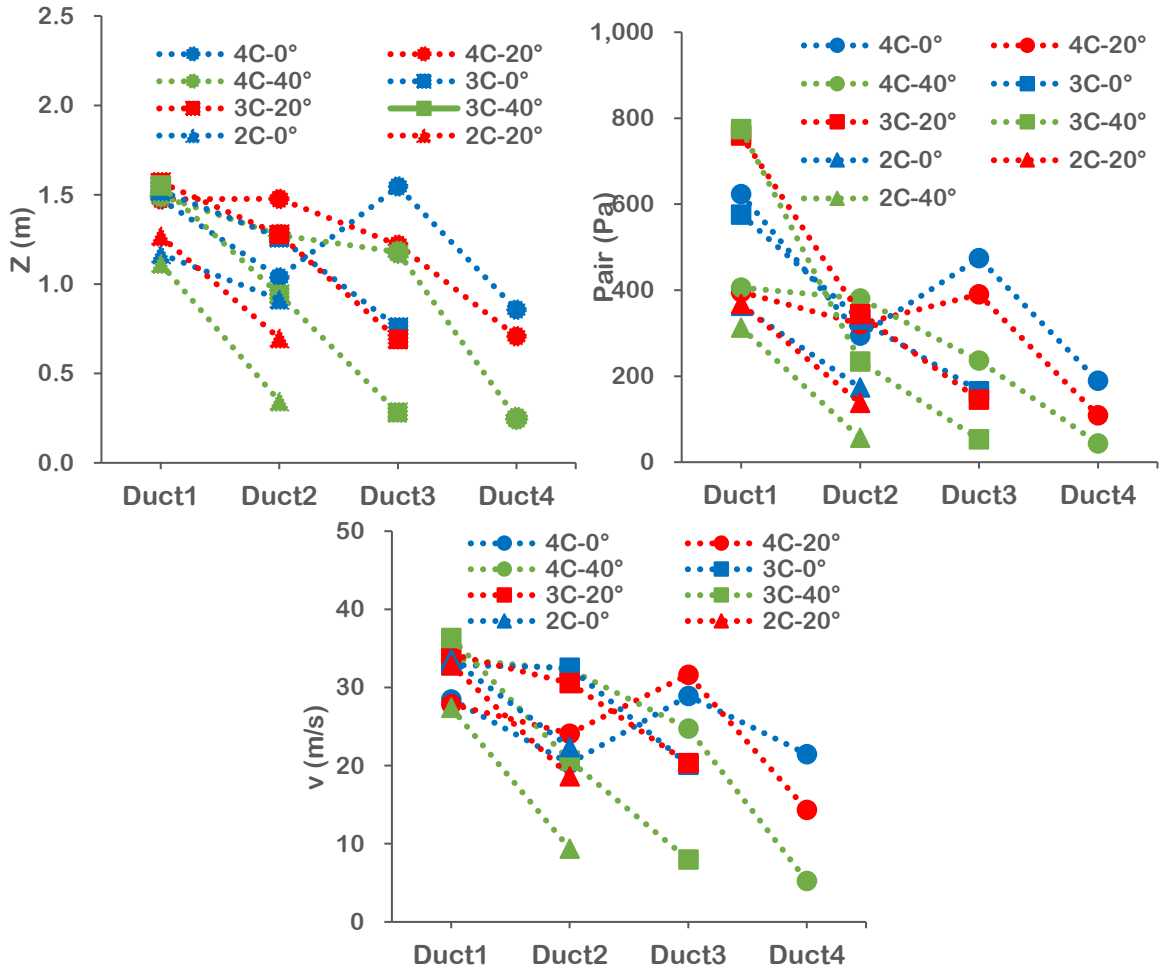

Fig. 7: The values of water level oscillation (Z), pressure (P), and air velocity (v)

value of 36.36 m/s. The lowest v is in Duct4 in the multi chamber model with an inclination of 40° with a value of 5.275 m/s.

Based on the number of chambers or ducts, in Figure 7 it can be seen that in general the values of water level oscillation (Z), pressure (P), and air velocity (v) tend to be lower than configurations with more chambers. In Figure 7(a), the water level oscillation (Z) in 2 ducts is more evenly distributed compared to additional ducts in 3 or 4 chamber configurations. In Figure 7(b), the addition of one chamber increases the complexity of airflow and pressure. The values of Z, P, and v show a more complex distribution compared to 2 chambers. The decrease in Duct3 is quite significant, indicating that the effect of additional ducts weakens the energy contribution from the last duct. Likewise in Figure 7(c), the more chambers, the values of Z, P, and v become more segmented. Pressure and air velocity are more concentrated in the first duct (Duct1), while the last duct (Duct4) has a relatively low value. The energy distribution appears less absorbed in the 4th duct because the values of Z, P, and v decrease drastically.

Based on the variation of inclination, in Figure 7 it can be seen that the Z value tends to decrease with increasing inclination (from 0° to 40°). This indicates that a larger inclination angle reduces the interaction of water and air, which affects the absorption of oscillation. In 4 chambers, the last duct (Duct4) has a Z that is almost close to zero at an inclination of 40°. Meanwhile, the pressure (P) shows a very high value in the first duct (Duct1), especially for an inclination of 0°. The pressure tends to decrease in the following ducts (Duct2, Duct3, and Duct4). At an inclination of 40°, the P value in Duct2 to Duct4 is very low, indicating a weaker energy distribution. The air velocity in the duct also decreases with increasing inclination. In the last duct (especially in 3 and 4 chambers), the velocity becomes very small at an inclination of 40°. At an inclination of 0°, the air velocity shows a more even energy distribution.

3.4. Comparative analysis of power distribution between ducts

Based on Table 2 it can be seen that at an inclination angle of 0°, the power is distributed relatively evenly with Duct1 (11.36 kW) and Duct3 (11.88 kW) dominant. Duct4 produces minimum power (4.86 kW). At 20°, the power increases in Duct3 (15.54 kW) but decreases drastically in Duct4 (1.45 kW). At 40°, Duct1 and Duct2 produce the highest power (18.77 and 16.51 kW), while Duct4 is

almost zero (0.07 kW). This can be interpreted as Duct3 tends to be dominant at low angles (0° and 20°), indicating a significant focus of airflow velocity towards this duct due to a more uniform pressure distribution in the chamber (see Figure 6a) . At 40°, the airflow velocity in Duct4 is very low, possibly because the air pressure distribution becomes not absorbed due to the steeper angle hindering the optimal oscillatory flow of water (see Figure 6b).

Based on Table 3 it can be seen that at an angle of 0°, the power is quite evenly distributed between Duct1 (17.45 kW) and Duct2 (16.91 kW), but Duct3 is much smaller (4.00 kW). At 20°, the power in Duct1 increases (19.74 kW) while Duct2 decreases slightly (14.02 kW). Duct3 is stable low (4.13 kW). At 40°, Duct1 produces the largest power (23.58 kW), but Duct2 and Duct3 decrease drastically (4.32 and 0.25 kW). This can be interpreted that in this configuration, the airflow velocity appears to be more focused on Duct1 with increasing angle (see Figure 5). This can be explained by the dominance of air pressure near this duct due to the pressure distribution that is more inclined to the side closest to the chamber (see the air pressure phenomenon in Figure 6b). Duct3 has the lowest absorption, probably because its position is not optimal for water oscillation.

Based on Table 4, it can be seen that at an angle of 0°, Duct1 produces more power (18.67 kW) than Duct2 (5.49 kW). At 20°, the power of Duct1 decreases slightly (17.45 kW) and Duct2 decreases drastically (3.18 kW). At 40°, Duct1 decreases further (10.10 kW), while Duct2 approaches zero (0.41 kW). This can be interpreted that in the 2-chamber configuration, the airflow velocity appears to be very focused on Duct1 (See Figure 5a). The decrease in power in Duct2 indicates that the airflow velocity and air pressure in the second chamber become very low at large angles (see the visualization of airflow velocity and air pressure in Figures 6a and 6b). Suboptimal water oscillation in the second chamber can also be the cause of poor pressure distribution.

Overall, in Tables 2, 3, and 4, it can be interpreted that smaller angles (0° and 20°) produce a more even distribution of airflow velocity because the water oscillation in the chamber is more stable. The air pressure tends to be higher overall, allowing higher power in all ducts. At an angle of 40°, the airflow velocity is focused on Duct1, while other ducts experience a significant decrease. This is due to the increased air turbulence and the disturbed water oscillation flow due to gravity and the inclined geometry. In addition, the 4-chamber configuration produces a more even power distribution at small angles, but its absorption decreases at large angles. This indicates that the airflow velocity and air pressure cannot be optimally utilized in ducts far from the oscillation source. The 2-chamber configuration produces dominant power in the nearest duct, but the second duct hardly contributes at large angles.

In terms of design implications, in tables 2, 3, and 4, it can be seen that an inclination angle of 20° is the best compromise, producing adequate power distribution across most ducts for all configurations. An inclination angle of 40° produces peak power in the dominant duct but renders the other ducts not absorbed. For multi-duct configurations, redistribution of air pressure with additional design features (e.g. air dividers or valve controls) can improve the absorption of the less dominant ducts. Adjusting the horizontal length of the chamber or inserting deflectors to increase water oscillation can help create more even pressure.

Table 2: Power distribution between ducts in 4 chambers

Inclination	Duct1	Duct2	Duct3	Duct4
0°	11.36	4.09	11.88	4.86
20°	10.64	6.88	15.54	1.45
40°	18.77	16.51	7.44	0.07

Table 3: Power distribution between ducts in 3 chambers

Inclination	Duct1	Duct2	Duct3
0°	17.45	16.91	4.00
20°	19.74	14.02	4.13
40°	23.58	4.32	0.25

Table 4: Power distribution between ducts in 2 chambers

Inclination	Duct1	Duct2
0°	18.67	5.49
20°	17.45	3.18
40°	10.10	0.41

3.5. Comparative analysis of power absorption

Based on Figure 8, there is a difference in the comparison of the multi chamber OWC power absorption from the interpretation of the inclination. When the configuration is 4 chambers, at an inclination of 0°, the power is at an intermediate level. When the inclination is 20°, there is an increase in power compared to 0°. At an inclination of 40°, the highest total power is generated in this configuration. From the interpretation results, the inclination of 40° shows an increase in the absorption of water oscillation and airflow, maximizing the pressure transmitted to the duct. The addition of the number of ducts allows for a more even pressure distribution at optimal water oscillation conditions (in Figure 6b).

When the 3-chamber configuration, at inclinations of 0° and 20°, the power generated is almost the same and higher than the 40° inclination. At an inclination of 40°, the power decreases significantly but is still at a moderate level. From the interpretation results, this configuration works better at low to medium inclinations (0° and 20°) because the fewer ducts provide greater pressure per duct. At inclination 40°, the absorption decreases because the combination of water

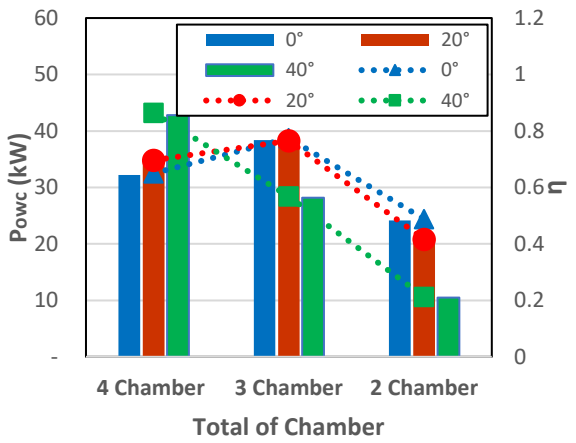

Fig. 8: Power absorption comparison chart of multi chamber OWC

oscillation and pressure distribution becomes less optimal compared to the 4-chamber configuration.

When the 2-chamber configuration, at inclinations of 0° and 20°, the power is lower than other configurations. At an inclination of 40°, the power is the lowest among all configurations. From the interpretation, with only 2 ducts, the total power generated is limited because the volume of air processed is smaller. At an inclination of 40°, the airflow and air pressure tend to be not absorbed, resulting in much lower power.

Based on the comparative analysis, three conclusions can be drawn, the highest absorption is found in the 4- chamber configuration, where at an inclination of 40° it produces the highest total power. This shows that large inclinations are more effective in designs with more ducts. Absorption at low inclination is found in the 3-chamber configuration which works optimally at 0° and 20°, which is superior to other configurations. This may be due to the more effective air pressure distribution with fewer ducts. The decrease in absorption in the chamber is found with a limited number of chambers and ducts, the total absorption decreases significantly, especially at an inclination of 40°.

For maximum power, a configuration with more chambers (such as 4 chambers) is better at high inclinations. For more uniform power at various inclinations, a 3-chamber configuration can be an effective choice as an optimal design. With only 2 chambers, the volume of water oscillation produced is smaller/limited compared to a 3 or 4 chamber configuration. Since the air pressure produced in each chamber depends on the volume of water oscillation, fewer chambers result in lower total pressure.

The efficiency analysis of multi-chamber OWC shows that 3 chambers are more optimal at 0° and 20°, while 4 chambers are more efficient at 40°. 2 chambers have the lowest efficiency, especially at higher inclinations. This trend suggests that 3 chambers perform better at smaller inclinations, whereas 4 chambers excel at larger angles due to more effective wave interactions. At 40°, 4 chambers achieve the highest efficiency (0.86), while 2 chambers experience a significant drop (0.21). For maximum efficiency, 4 chambers at 40° are recommended. However, for a balance between efficiency and a simpler design, 3 chambers at 0° or 20° are more optimal.

In a multi chamber system, the air pressure from the chamber must be distributed to the ducts. With fewer chambers, the pressure distribution becomes uneven, making the airflow to the ducts less absorbed in distributing pressure. In a 2-chamber configuration, each duct tends to receive less pressure, especially at high inclination angles. The interaction between the water oscillations in the two chambers is more difficult to synchronize than in three or four chambers. This causes hydrodynamic losses where the internal waves in the chambers are less effective in generating air pressure

The single chamber system has the advantage that it will have a focused oscillation. Because there is no interaction between chambers, the resulting air pressure can be more stable and directed. This is simpler in design and may be suitable for scenarios with small duct sizes or airflow focused on one generator. The disadvantage of a single chamber is that the total volume of water oscillation is very limited, so the maximum power produced is much lower than a multi chamber configuration. The inclination angle has a significant impact because, with only one chamber, angle variations can directly affect the efficiency of airflow and pressure[63)]

There is an influence of angle on hydrodynamics/ airflow velocity with an inclination angle of 0°, an inclination angle of 20°, and an inclination angle of 40°. High inclination angles (40°) increase the air pressure in a particular duct because the airflow is more concentrated due to the steep slope. However, if the pressure is uneven or the duct is not designed to handle high pressure, this can cause stagnation or turbulence in a particular duct. At low inclinations (0° and 20°), the airflow tends to be more stable and laminar, resulting in higher airflow absorption in the duct. At high inclinations (40°), the airflow often becomes turbulent, which can reduce energy conversion absorption (see Figures 6a and 6b).

There is an influence of angle on hydrodynamics/ airflow velocity with an inclination angle of 0°, an inclination angle of 20°, and an inclination angle of 40°. High inclination angles (40°) increase the air pressure in a particular duct because the airflow is more concentrated due to the steep slope. However, if the pressure is uneven or the duct is not designed to handle high pressure, this can cause stagnation or turbulence in a particular duct. At low inclinations (0° and 20°), the airflow tends to be more stable and laminar, resulting in higher airflow absorption in the duct. At high inclinations (40°), the airflow often becomes turbulent, which can reduce energy conversion absorption (see Figures 6a and 6b).

The study by Lino et al. (2016) showed that changes in motion direction in an inclined OWC significantly affect

oscillation characteristics, particularly by extending the resonance period, which is a crucial factor in OWC design[68]. These findings align with this research, where the chamber inclination in a multi-chamber OWC influences wave power extraction efficiency. The inclination of the chamber can alter airflow dynamics and pressure within the system, contributing to the overall performance of the OWC.

The study by Zhao et al. (2021) showed that the hydrodynamic interaction between chambers in a multi-chamber OWC enhances wave power extraction efficiency, optimizing pressure distribution and airflow[69]. These findings align with my research, where adding chambers optimizes pressure distribution and airflow, enabling more effective energy conversion and improving the overall performance of the OWC system[70].

4. Conclusions and Recommendations

Based on the results of this study, the performance of multi-chamber Oscillating Water Column (OWC) configurations varies significantly depending on the number of chambers and the inclination angle. The maximum free surface elevation (Z) of 1.545 meters was observed in the 4-chamber configuration (Duct3) with a 0° inclination. The highest air pressure (774.804 Pa) and air velocity (36.356 m/s) were both recorded in the 3-chamber configuration (Duct1) with a 40° inclination.

In terms of energy output, the maximum power distribution reached 23.58 kWh in the 3-chamber, 40° inclined duct (Duct1), while the lowest output was 0.07 kWh in the 4-chamber, 40° inclined duct (Duct4). The highest total power absorption of 42.79 kWh was achieved in the 4-chamber configuration with a 40° inclination, which also exhibited the highest system efficiency of 86%. The results indicate that increasing the number of chambers generally enhances the performance of the OWC system in terms of pressure and air velocity. However, performance is often concentrated in the first duct (Duct1), while the last duct (Duct4) contributes less, especially at steeper inclinations. The water level oscillation (Z) decreases as the inclination increases from 0° to 40°, which reduces the air-water interaction and diminishes energy transfer.

This study provides a solid foundation for future research in hydrodynamics and wave energy conversion, with several aspects remaining open for further investigation to enhance system performance and understanding. Key areas include optimizing duct and chamber configurations, analyzing the effects of varying wave periods (T) and water heights (H), and evaluating system performance under irregular wave conditions or real-sea simulations. These efforts are essential to improve efficiency, reliability, and the practical applicability of wave energy conversion technologies. These directions could lead to more optimized OWC designs for practical and scalable energy harvesting applications.

Acknowledgements

This research was supported by funding from the Renewable Energy Program House - OREM of the National Research and Innovation Agency (BRIN) under the 2024 grant scheme, Grant Number B-12293/III.3/HM.07.00/11/2023

Nomenclature

A	wave amplitude (m)
c	wave velocity (m/s)
fm	volume fraction (–)
g	acceleration due to gravity (m/s2)
h	water depth (m)
P	air pressure (Pa)
t	time (s)
U	velocity field (m/s)
v	air velocity (m/s)
Z	water level oscillation (m)
Greek symbols	
ω	wave frequency (Hz)
λ	wavelength (m)
ρ	fluid density (kg/m^3)
∇	laplacian vector (–)
μ	dynamic viscosity (Pa.s)
φ	phase shift angle (–)
Subscript	
0	water
1	air

References

1) Arief Heru Kuncoro, Joko Santosa, Ira Fitriana, Agus Nurrohim, Agus Sugiyono, Slamet, Euis Djubaedah, Vetri Nurliyanti, Nona Niode, and Prima Trie Wijaya, "Towards net zero emission in indonesia: strategic fuel demand analysis for sustainable electricity (2022-2060)," Evergreen, 11 (4) 3606–3617 (2024). doi:10.5109/7326993.

2) Muhammad Alfan Santoso, Y. Wijayanti, Ridwan Budi Prasetyo, O. Setyandito, Nizam, Aprijanto, A. Subandriya, Aries Taufiq Kurniawan, A. Sudaryanto, and B. Sutejo, "A mini review: wave energy converters technology, potential applications and current research in indonesia," Evergreen, 10 (3) 1642–1650 (2023). doi:10.5109/7151712.

3) A.M.M. Ismaiel, and S. Yosida, "Study of turbulence intensity effect on the fatigue lifetime of wind turbines," Evergreen, 5 (1) 25–32 (2018). doi:10.5109/1929727.

4) Raed A. Jessam, "Experimental study of wind turbine power generation utilizing discharged air of air conditioner blower," Evergreen, 9 (4) 1103–1109

(2022). doi:10.5109/6625722.

5) P. Byrne, N. Putra, T. Maré, N. Abdallah, P. Lalanne, I. Alhamid, P. Estelle, A. Yatim, and A.-L. Tiffonnet, "Design of a solar ac system including a pcm storage for sustainable resorts in tropical region," Evergreen, 6 (2) 143–148 (2019). doi:10.5109/2321009.
6) I. Roihan, Kynan Tjandaputra A., Eko A. Setiawan, and Raldi A. Koestoer, "Installing and testing the grashof portable incubator powered using the solar box 'be-care' for remote areas without electricity," Evergreen, 7 (4) 621–628 (2020). doi:10.5109/4150516.
7) H.A. Jaffar, A.A. Ismaeel, and Ahlam Luaibi Shuraiji, "Review of hybrid photovoltaic- air updraft solar application: present and proposed state models," Evergreen, 9 (4) 1181–1202 (2022). doi:10.5109/6625729.
8) B.T. Prasetyo, Suyanto, M. Oktaufik, and S. Himawan, "Design, construction and preliminary test operation of bppt-3MW condensing turbine geothermal power plant," Evergreen, 6 (2) 162–167 (2019). doi:10.5109/2321012.
9) Y. Gunawan, N. Putra, E. Kusrini, Imansyah Ibnu Hakim, and Muhamad Dicky Hans Setiawan, "Study of heat pipe utilizing low-temperature geothermal energy and zeolite-a for tea leaves withering process," Evergreen, 7 (2) 221–227 (2020). doi:10.5109/4055223.
10) I. López, J. Andreu, S. Ceballos, I. Martínez De Alegría, and I. Kortabarria, "Review of wave energy technologies and the necessary power-equipment," Renewable and Sustainable Energy Reviews, 27 413–434 (2013). doi:10.1016/j.rser.2013.07.009.
11) L.Y. Kai, S. Sarip, H.M. Kaidi, J.A. Ardila-Rey, N.M. Samsuddin, M.N. Muhtazaruddin, F. Muhammad-Sukki, and S.A. Aziz, "Current status and possible future applications of marine current energy devices in malaysia: a review," IEEE Access, 9 86869–86888 (2021). doi:10.1109/ACCESS.2021.3088761.
12) T.K. Das, P. Halder, and A. Samad, "Optimal design of air turbines for oscillating water column wave energy systems: a review," The International Journal of Ocean and Climate Systems, 8 (1) 37–49 (2017). doi:10.1177/1759313117693639.
13) Masuda, Y. "Performance Optimization of A Pneumatic Wave Energy Conversion Device (U)" Naval Academy Annapolis, Maryland, Midshipman Stephen W. Surko, 1/C 26 AUG 82 U.S.N.A.-TPR-120. Trident Scholar project report; no. 120 (1982).
14) M. Suzuki, C. Arakawa, and S. Takahashi, "Performance of Wave Power Generating System Installed In Breakwater At Sakata Port In Japan," Paper presented at the The Fourteenth International Offshore and Polar Engineering Conference, Toulon, France, Paper Number: ISOPE-I-04-137 (2004). ISBN 1-880653-62-1 (Set); ISSN 109806189.
15) A.F.O. Falcão, and J.C.C. Henriques, "Oscillating-water-column wave energy converters and air turbines: a review," Renewable Energy, 85 1391–1424 (2016). doi:10.1016/j.renene.2015.07.086.
16) D. Zhang, W. Li, and Y. Lin, "Wave energy in china: current status and perspectives," Renewable Energy, 34 (10) 2089–2092 (2009). doi:10.1016/j.renene.2009.03.014.
17) Chenhua Ni, "Development of ocean energy test field in china," JSOE, 5 (1) (2015). doi:10.17265/2159-5879/2015.01.005.
18) M. Ravindran and Paul Mario Koola, "Energy From Sea Waves—The Indian Wave Energy Programme," Current Science, Vol. 60, No. 12 676–680. Current Science Association. 25 June 1991. URL https://www.jstor.org/stable/24093688.
19) A. Thakker, F. Hourigan, T.S. Dhanasekaran, M.El. Hemry, Z. Usmani, and J. Ryan, "Design and performance analysis of impulse turbine for a wave energy power plant," Int. J. Energy Res., 29 (1) 13–36 (2005). doi:10.1002/er.1034.
20) K. Mala, and J. Jayaraj, "Performance comparison of power modules in the indian wave energy plant," Proceedings of The Eighth The International Society of Offshore and Polar Engineers (ISOPE) Ocean Mining Symposium Chennai, India, September 20-24, 2009. ISBN 978-1-880653-75-3; ISSN 1946-0066.
21) Y. Washio, H. Osawa, and T. Ogata, "The open sea tests of the offshore floating type wave power device 'Mighty Whale' -characteristics of wave energy absorption and power generation," in: MTS/IEEE Oceans 2001. An Ocean Odyssey. Conference Proceedings (IEEE Cat. No.01CH37295), Marine Technol. Soc, Honolulu, HI, USA, 2001: pp. 579–585. doi:10.1109/OCEANS.2001.968786.
22) A. Clément, P. McCullen, A. Falcão, A. Fiorentino, F. Gardner, K. Hammarlund, G. Lemonis, T. Lewis, K. Nielsen, S. Petroncini, M.-T. Pontes, P. Schild, B.-O. Sjöström, H.C. Sørensen, and T. Thorpe, "Wave energy in europe: current status and perspectives," Renewable and Sustainable Energy Reviews, 6 (5) 405–431 (2002). doi:10.1016/S1364-0321(02)00009-6.
23) M. Takao, E. Sato, S. Nagata, K. Toyota, and T. Setoguchi, "A Sea Trial of Wave Power Plant With Impulse Turbine," in: Volume 6: Nick Newman Symposium on Marine Hydrodynamics; Yoshida and Maeda Special Symposium on Ocean Space Utilization; Special Symposium on Offshore Renewable Energy, ASMEDC, Estoril, Portugal, 2008: pp. 681–688. doi:10.1115/OMAE2008-57535.
24) M. Suzuki, M. Takao, E. Satoh, S. Nagata, K. Toyota, and T. Setoguchi, "Performance prediction of owc

type small size wave power device with impulse turbine," JFST, 3 (3) 466–475 (2008). doi:10.1299/jfst.3.466.

25) R. Alcorn, A. Blavette, M. Healy, and A. Lewis, "FP7 eu funded cores wave energy project: a coordinators' perspective on the galway bay sea trials," Uw Tech: Int j Soc Uw Tech, 32 (1) 51–59 (2014). doi:10.3723/ut.32.051.
26) Y. Torre-Enciso, and I. Ortubia, "Mutriku wave power plant: from the thinking out to the reality," Proceedings of the 8th European Wave and Tidal Energy Conference, Uppsala, Sweden, 2009.
27) T.J.T. Whittaker, D. Langston, N. Fletcher, and A.F. de O. Falcao, "ISLAY limpet wave power plant," Publishable Report Research funded in part by The European Commission In the framework of the Non Nuclear Energy Programme Joule III. 2002.
28) F. Arena, A. Romolo, G. Malara, and A. Ascanelli, "On Design and Building of a U-OWC Wave Energy Converter in the Mediterranean Sea: A Case Study," in: Volume 8: Ocean Renewable Energy, American Society of Mechanical Engineers, Nantes, France, 2013: p. V008T09A102. doi:10.1115/OMAE2013-11593.
29) F. Arena, V. Fiamma, R. Iannolo, V. Laface, G. Malara, A. Romolo, and F.M. Strati, "Resonant wave energy converters: small-scale field experiments and first full-scale prototype," Energia, Ambiente e Innovazione, (Speciale II 2015) 58–67 (2015). doi:10.12910/EAI2015-046.
30) Z. Liu, B. Hyun, J. Jin, K. Hong, and Y. Lee, "OWC air chamber performance prediction under impulse turbine damping effects," Sci. China Technol. Sci., 59 (4) 657–666 (2016). doi:10.1007/s11431-016-6030-5.
31) D.H. Yacob, S. Sarip, H.M. Kaidi, J.A. Ardila-Rey, and F. Muhammad-Sukki, "Oscillating water column geometrical factors and system performance: a review," IEEE Access, 10 32104–32122 (2022). doi:10.1109/ACCESS.2022.3160713.
32) N. Portillo Juan, V. Negro Valdecantos, M.D. Esteban, and J.S. López Gutiérrez, "Review of the influence of oceanographic and geometric parameters on oscillating water columns," JMSE, 10 (2) 226 (2022). doi:10.3390/jmse10020226.
33) I. López, R. Carballo, D.M. Fouz, and G. Iglesias, "Design selection and geometry in owc wave energy converters for performance," Energies, 14 (6) 1707 (2021). doi:10.3390/en14061707.
34) D. Ning, Y. Zhou, R. Mayon, and L. Johanning, "Experimental investigation on the hydrodynamic performance of a cylindrical dual-chamber oscillating water column device," Applied Energy, 260 114252 (2020). doi:10.1016/j.apenergy.2019.114252.
35) X.L. Zhao, D.Z. Ning, Q.P. Zou, D.S. Qiao, and S.Q. Cai, "Hybrid floating breakwater-wec system: a review," Ocean Engineering, 186 106126 (2019). doi:10.1016/j.oceaneng.2019.106126.
36) D. Ning, Y. Zhou, and C. Zhang, "Hydrodynamic modeling of a novel dual-chamber owc wave energy converter," Applied Ocean Research, 78 180–191 (2018). doi:10.1016/j.apor.2018.06.016.
37) A. Elhanafi, G. Macfarlane, and D. Ning, "Hydrodynamic performance of single–chamber and dual–chamber offshore–stationary oscillating water column devices using cfd," Applied Energy, 228 82–96 (2018). doi:10.1016/j.apenergy.2018.06.069.
38) D.G. Dorrell, M.-F. Hsieh, and C.-C. Lin, "A multichamber oscillating water column using cascaded savonius turbines," IEEE Trans. on Ind. Applicat., 46 (6) 2372–2380 (2010). doi:10.1109/TIA.2010.2072979.
39) R. Wang, D. Ning, and Q. Zou, "Wave loads on a land-based dual-chamber oscillating water column wave energy device," Coastal Engineering, 160 103744 (2020). doi:10.1016/j.coastaleng.2020.103744.
40) J.U. Jasron, S. Soeparmani, L. Yuliati, and D.B. Darmadi, "Comparison of the performance of oscillating water column devices based on arrangements of water columns," JMES, 14 (3) 7082–7093 (2020). doi:10.15282/jmes.14.3.2020.10.0555.
41) J. Gadelho, K. Rezanejad, and C. Guedes Soares, "Experimental and numerical analysis of multi-chamber oscillating water column devices," J Hydrodyn, 36 (3) 492–503 (2024). doi:10.1007/s42241-024-0043-5.
42) P. Koirala, S. Nagata, Y. Imai, T. Murakami, and T. Setoguchi, "A numerical study on multi-chamber oscillating water columns," Journal of JSCE, 3 (1) 93–104 (2015). doi:10.2208/journalofjsce.3.1_93.
43) C. Wang, Z. Deng, P. Wang, and Y. Yao, "Wave power extraction from a dual oscillating-water-column system composed of heave-only and onshore units," Energies, 12 (9) 1742 (2019). doi:10.3390/en12091742.
44) A. Abbasnia, K. Rezanejad, and C. Guedes Soares, "Adaptive fully nonlinear potential model for the free surface under compressible air pressure of oscillating water column devices," Engineering Analysis with Boundary Elements, 133 153–164 (2021). doi:10.1016/j.enganabound.2021.08.018.
45) M. Shalby, A. Elhanafi, P. Walker, and D.G. Dorrell, "CFD modelling of a small–scale fixed multi–chamber owc device," Applied Ocean Research, 88 37–47 (2019). doi:10.1016/j.apor.2019.04.003.
46) J.F.M. Gadelho, and C. Guedes Soares, "CFD study of a dual chamber floating oscillating water column

device," Ocean Engineering, 261 111817 (2022). doi:10.1016/j.oceaneng.2022.111817.

47) J.-S. Kim, B.W. Nam, S. Kim, J. Park, S. Park, and K.-H. Kim, "Experimental study on hydrodynamic behavior and energy conversion of multiple oscillating-water-column chamber in regular waves," Ocean Engineering, 280 114495 (2023). doi:10.1016/j.oceaneng.2023.114495.
48) D. Ning, L. Fu, Y. Zhou, R. Mayon, and Y. Zhang, "Hydrodynamic performance of a land-based multi-chamber owc wave energy capture system: an experimental study," Coastal Engineering, 190 104510 (2024). doi:10.1016/j.coastaleng.2024.104510.
49) E. Supriyanto, A.T. Rohman, A.I. Malakani, I.Y. Ikhsanudin, A. Wibowo, M.T. Suryantoro, A. Musthofa, R.T. Soewono, M.P. Helios, A.D. Nugraha, Deendarlianto, and A.S.D. Marta, "Experimental study of flow characteristics in hydrodynamic and aerodynamic l-shaped and u-shaped oscillating water column chambers," Results in Engineering, 25 103762 (2025). doi:10.1016/j.rineng.2024.103762.
50) K. Rezanejad, J.F.M. Gadelho, and C. Guedes Soares, "Hydrodynamic analysis of an oscillating water column wave energy converter in the stepped bottom condition using cfd," Renewable Energy, 135 1241–1259 (2019). doi:10.1016/j.renene.2018.09.034.
51) K. Rezanejad, A. Souto-Iglesias, and C. Guedes Soares, "Experimental investigation on the hydrodynamic performance of an l-shaped duct oscillating water column wave energy converter," Ocean Engineering, 173 388–398 (2019). doi:10.1016/j.oceaneng.2019.01.009.
52) Y.-S. Kuo, C.-Y. Chung, S.-C. Hsiao, and Y.-K. Wang, "Hydrodynamic characteristics of oscillating water column caisson breakwaters," Renewable Energy, 103 439–447 (2017). doi:10.1016/j.renene.2016.11.028.
53) Z. Liu, C. Xu, K. Kim, J. Choi, and B. Hyun, "An integrated numerical model for the chamber-turbine system of an oscillating water column wave energy converter," Renewable and Sustainable Energy Reviews, 149 111350 (2021). doi:10.1016/j.rser.2021.111350.
54) V. Yakhot, and S.A. Orszag, "Renormalization group analysis of turbulence. i. basic theory," J Sci Comput, 1 (1) 3–51 (1986). doi:10.1007/BF01061452.
55) F. Opoku, M.N. Uddin, and M. Atkinson, "A review of computational methods for studying oscillating water columns – the navier-stokes based equation approach," Renewable and Sustainable Energy Reviews, 174 113124 (2023). doi:10.1016/j.rser.2022.113124.
56) M.R. Kavian Nezhad, C.F. Lange, and B.A. Fleck, "Performance evaluation of the rans models in predicting the pollutant concentration field within a compact urban setting: effects of the source location and turbulent schmidt number," Atmosphere, 13 (7) 1013 (2022). doi:10.3390/atmos13071013.
57) D. del O. Díaz, and D.F. Hinz, "Performance of eddy-viscosity turbulence models for predicting swirling pipe-flow: simulations and laser-doppler velocimetry," (2015). doi:10.48550/arXiv.1507.04648.
58) H.-L. Wu, S.-C. Hsiao, and T.-C. Lin, "Evolution of a two-layer fluid for solitary waves propagating over a submarine trench," Ocean Engineering, 110 36–50 (2015). doi:10.1016/j.oceaneng.2015.10.004.
59) T. Vyzikas, S. Deshoulières, O. Giroux, M. Barton, and D. Greaves, "Numerical study of fixed oscillating water column with rans-type two-phase cfd model," Renewable Energy, 102 294–305 (2017). doi:10.1016/j.renene.2016.10.044.
60) Z. Liu, B.-S. Hyun, and K. Hong, "Numerical study of air chamber for oscillating water column wave energy convertor," China Ocean Eng, 25 (1) 169–178 (2011). doi:10.1007/s13344-011-0015-8.
61) "Flow_Science_FLOW-3d_v9.3_user_manual _volume_1," Flow Science, Inc. Copyright 2008.
62) K. Trivedi, A.R. Ray, P.A. Krishnan, S. Koley, and T. Sahoo, "Hydrodynamics of an owc device in irregular incident waves using rans model," Fluids, 8 (1) 27 (2023). doi:10.3390/fluids8010027.
63) A.S.D. Marta, Deendarlianto, Indarto, Sarjiya, S. Kamal, and E. Winata, "Performance of OWC-Type Wave Power Plants in the Waters of Sumbawa Island, Indonesia," in: 2024 International Conference on Technology and Policy in Energy and Electric Power (ICTPEP), IEEE, Bali, Indonesia, 2024: pp. 415–420. doi:10.1109/ICT-PEP63827.2024.10733542.
64) Adnan Sandy Dwi Marta, Deendarlianto, W. Kongko, Aprijanto, Ahmad Taufiqur Rohman, A. Wibowo, and Irfan Yahya Ikhsanudin, "The influence of wave characteristics, tides, and installation conditions of l-shaped owc wave energy converter on energy absorption capability," Evergreen, 11 (3) 2607–2617 (2024). doi:10.5109/7236900.
65) Adnan Sandy Dwi Marta, Deendarlianto, W. Kongko, Indarto, Fauzun, and A.T. Rohman, "The influence of wave height and period on airflow velocity and differential pressure in l-shaped oscillating water column (l-owc) chamber for wave energy converter (wec)," Asia-Pacific Journal of Science and Technology, 29 5 (13 pages) (2024). doi:10.14456/APST.2024.90.
66) C. Wang, Y. Zhang, and Z. Deng, "Theoretical analysis on hydrodynamic performance for a dual-chamber oscillating water column device with a pitching front lip-wall," Energy, 226 120326 (2021).

doi:10.1016/j.energy.2021.120326.

67) J. Chen, H. Wen, Y. Wang, and G. Wang, “A correlation study of optimal chamber width with the relative front wall draught of onshore owc device,” Energy, 225 120307 (2021). doi:10.1016/j.energy.2021.120307.

68) M. Iino, T. Miyazaki, H. Segawa, and M. Iida, “Effect of inclination on oscillation characteristics of an oscillating water column wave energy converter,” Ocean Engineering, 116 226–235 (2016). doi:10.1016/j.oceaneng.2016.03.014.

69) X. Zhao, L. Zhang, M. Li, and L. Johanning, “Experimental investigation on the hydrodynamic performance of a multi-chamber owc-breakwater,” Renewable and Sustainable Energy Reviews, 150 111512 (2021). doi:10.1016/j.rser.2021.111512.

70) X. Zhao, J. Zhou, Z. Wang, Q. Zou, and E. Renzi, “Hydrodynamic performance of multi-chamber oscillating water columns in a caisson array,” Energy, 305 132217 (2024). doi:10.1016/j.energy.2024.132217.